Rapid and Scalable Reduction of Dense Surface-Supported Metal-Oxide Catalyst with Hydrazine Vapor

Cary L. Pint,[†,§] Seung Min Kim,[∥] Eric A. Stach,[∥] and Robert H. Hauge[‡,§,*]

[†]Department of Physics and Astronomy, [‡]Department of Chemistry, [§]Richard E. Smalley Institute for Nanoscale Science and Technology, Rice University, Houston, Texas 77251, and [∥]School of Materials Engineering and Birck Nanotechnology Center, Purdue University, West Lafayette, Indiana 47907

ABSTRACT An efficient technique using hydrazine (N_2H_4) vapor as an agent for the rapid reduction of high-density layers of catalytic nanoparticles is demonstrated. With as little as 10 mTorr hydrazine bled into a thermal chemical vapor deposition (CVD) apparatus, efficient reduction of metal-oxide catalyst particles is achieved more rapidly than when using atomic hydrogen as the reducing agent. Postreduction catalyst imaging emphasizes the differences in nanoparticle formation under different reduction environments, with the most uniform and compact catalyst size distribution observed following hydrazine exposure. Low-temperature reduction studies suggest that as little as 15 s N_2H_4 exposure at temperatures of 350 °C can yield a reduced catalyst layer preceding the synthesis of dense, aligned arrays of single-walled carbon nanotubes (SWNT) with uniform height. This work demonstrates a simple route toward scalable, vapor transport reduction of metal-oxide catalyst relevant to a number of catalytic applications, including the synthesis and selective synthesis of aligned SWNT arrays.

KEYWORDS: hydrazine · catalysis · carbon nanotubes · chemical vapor deposition

The synthesis of a variety of nanostructured materials possessing unique and exciting physical properties has been the foundation for the development of new and important applications based upon nanotechnology. Of the many such nanostructures that fit into this category, nanorods and nanowires composed of Si[1−4] and ZnO,[5] as well as nanotubes composed of BN[6] and C,[7−13] have emerged as premier candidates for the future of developing applications. Despite the fact that each of these nanostructures is unique in the properties that make it attractive for such applications, all of these structures can be synthesized in a universal process that utilizes vapor transport at elevated temperatures with metallic catalytic nanoparticles. In many cases, where the catalyst forms a stable metal-oxide when exposed to ambient conditions, the first stage of this process involves the reduction or preparation of a metal-oxide catalyst into a catalytically active metallic state. This is a highly crucial step in any process where selectivity in the catalyst particle size is sought (particularly for single-walled carbon nanotubes) since dynamic behavior of metal atoms on a supporting surface can limit control of the resulting particle size distribution.[14−17] This is a substantial issue that is particularly relevant for the nucleation and growth of dense arrays of single-walled carbon nanotubes, where the typical metal catalyst particle is less than 5 nm in diameter, with interparticle spacing of less than 10 nm on the solid oxide supporting surface.[17] As a result, the route toward selectivity in any high-density surface-supported growth process will require the ability to reduce the catalyst without initiating any coarsening of the catalyst particles prior to growth. This is a difficult task since most techniques which utilize a vapor transport growth process require a high pressure background level of H_2 at elevated temperatures (>700 °C) prior to the introduction of the reactive feedstock species in order to achieve a metallic catalyst state.[18] Recent work by Nessim *et al.*[16] has shown that varying the time of reduction in the pretreatment of Al_2O_3-supported Fe catalyst allows one to tailor the catalyst particle size distribution (and hence, nanotube diameter) in vertically aligned carbon nanotube array growth based upon catalyst coarsening. Although this technique can be used as a tool for selectivity of carbon nanotube growth by diameter and number of walls, it also highlights the sensitivity of the catalyst to the reduction conditions utilized in most similar chemical vapor deposition techniques.

Therefore, the route toward selectivity and controllability in catalysis is to utilize a reduction step which can be efficiently applied to a metal-oxide catalyst for as briefly as possible and at the lowest temperature possible. In this spirit, the development of the hot filament technique in CVD carbon

*Address correspondence to hauge@rice.edu.

Received for review March 6, 2009 and accepted May 27, 2009.

Published online June 1, 2009.
10.1021/nn900225h CCC: $40.75

nanotube growth[12,13,19] provides a simple route toward this goal as the use of a hot filament promotes the production of atomic hydrogen in the presence of H_2. Since atomic hydrogen is a highly efficient reducing agent of metal-oxides, rapid catalyst activation is achieved while minimizing effects such as coarsening in the first stage of this process. However, despite this advantage, the primary drawback to using the hot filament is tied to the finite diffusion distance of atomic hydrogen once it is produced. This limits the surface area over which uniform reduction occurs in a hot filament CVD apparatus and leads to nonuniformity in the reduction of large surfaces. Furthermore, the number of applications involving vertically aligned carbon nanotube arrays is rising at a remarkable rate—including supercapacitors,[20] field emitters,[21] filtration membranes,[22,23] and even films drawn from arrays that can be used as loudspeakers.[24] This rising number of applications emphasizes the concept that methods which can controllably promote selective and scalable growth are of utmost importance as the demand for processes to mass produce materials for these applications becomes greater.

In this study, we demonstrate a technique for metal-oxide catalyst reduction that appears more efficient than any other vapor transport reduction technique, utilizing brief exposures of hydrazine gas to an iron-oxide catalyst layer. With exposures as short as 3 s, and with as little as 10 mTorr partial pressure of hydrazine, catalyst reduction is attained and uniform growth can proceed from the catalytic layer. Compared to reduction with a hot filament, hydrazine vapor is more effective for reduction at lower temperatures and is more scalable in its ability to form highly uniform arrays of carbon nanotubes with a height invariant relative to the position of the chip in the heated furnace. The results of this study emphasize a route toward scalable and selective growth processes for future CVD reactor systems—not only for carbon nanotube growth but also for any CVD growth process which requires or benefits from the use of a metallic catalytic particle.

RESULTS AND DISCUSSION

The use of hydrazine reduction in this study is developed as a means to scale-up a low-pressure vapor transport system for growing single-walled carbon nanotube (SWNT) arrays, as an alternative to the use of high-pressure hydrogen reduction or low-pressure atomic hydrogen reduction. Hydrazine reduction of metal-oxide catalyst is achieved through a simple apparatus design that is illustrated in a cartoon in Figure 1 and discussed in further detail in the Methods and Supporting Information. The principle of utilizing this design is based upon the introduction of a well-known and controllable amount of hydrazine into a vapor transport reactor based

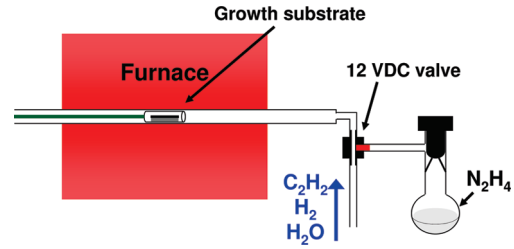

Figure 1. Simple schematic of the experimental setup utilized for N_2H_4 introduction to the reactor system. A photograph of the actual setup is included in the Supporting Information.

on the equilibrium vapor pressure of hydrazine under vacuum. To achieve this, an evacuated flask containing hydrazine is connected through a two-way solenoid valve that, when opened, allows hydrazine vapor to mix with the other reaction gases (C_2H_2, H_2, H_2O). The partial pressure of hydrazine in the vicinity of the metal-oxide catalyst can be carefully controlled by an O-ring fitting that modifies the opening of the hydrazine flask to the two-way valve. To achieve a low equilibrium pressure of hydrazine, the O-ring fitting can be only slightly opened, whereas the greatest hydrazine partial pressure can be achieved (~0.5 Torr) when the fitting on the hydrazine-containing flask is completely open to the two-way valve. An alternative technique to controllably introduce hydrazine is to utilize a temperature-controlled bath and follow the temperature dependence of the equilibrium vapor pressure of hydrazine to maintain a controllable N_2H_4 partial pressure. Nonetheless, for the experiments reported in this study, the process of modifying the opening of the O-ring fitting on the hydrazine flask is sufficient, allowing us to achieve hydrazine partial pressures between 10 and 500 mTorr.

In order to assess the effect of hydrazine reduction, we first focus on the lowest N_2H_4 partial pressures achievable during catalyst reduction and the effect of this on the growth of dense arrays of SWNTs. In a thermal CVD reactor operating at low pressures utilizing only H_2 (no atomic hydrogen or N_2H_4) as the reducing agent, the reduction and growth is poor. This is evidenced through a scanning electron microscope (SEM) image shown in Figure 2a. Not only does growth occur

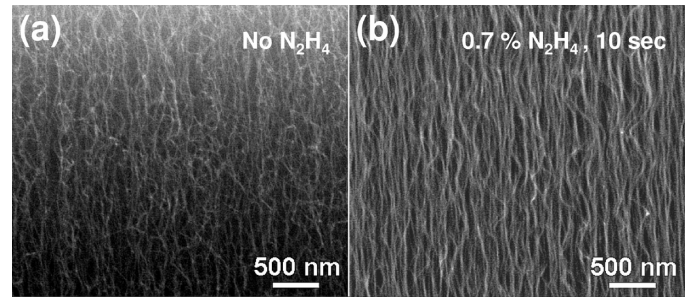

Figure 2. Side-view SEM images of SWNT forests grown with (a) only H_2 (1.4 Torr) for reduction, and (b) an additional 10 mTorr of N_2H_4 for 10 s of reduction upon rapid sample insertion into the furnace, at 750 °C in identical conditions.

nonuniformly over the whole chip (preferentially on edges), but the resulting growth looks much more "forest-like" as opposed to being composed of dense, aligned SWNT arrays. In order to combat this, most efforts to achieve uniform, high-density growth of SWNT arrays utilize an atmospheric process which results in rapid H_2 reduction of a metal-oxide catalyst. The setback to such a system is the extreme difficulty in achieving reproducible growth conditions in addition to the sensitive nature of atmospheric water-assisted SWNT forest growth. This has led to the development of hot filament reduction producing atomic hydrogen for aligned SWNT growth, which is a common technique utilized in CVD diamond growth.[25] However, this also has limits since the reduction process crucially depends on the distance of the catalyst surface from the hot filament. On the other hand, utilizing a reduction technique such as hydrazine is not spatially limited and can be just as easily applied to a large-area growth surface as a small research-scale substrate. Furthermore, N_2H_4 is a highly aggressive reducing agent, leading to uniform catalyst reduction at low N_2H_4 partial pressure following a brief exposure at high temperature (600−750 °C). Figure 2b shows an SEM image of a SWNT array grown following a 10 s reduction at 750 °C with only 10 mTorr partial pressure of N_2H_4 (0.7% of the total reaction mixture). Not only does the growth proceed in a remarkably uniform fashion over the growth substrate, but the height, alignment, density, and appearance of the SWNT array are comparable to an array grown with a 30 s exposure to atomic hydrogen.

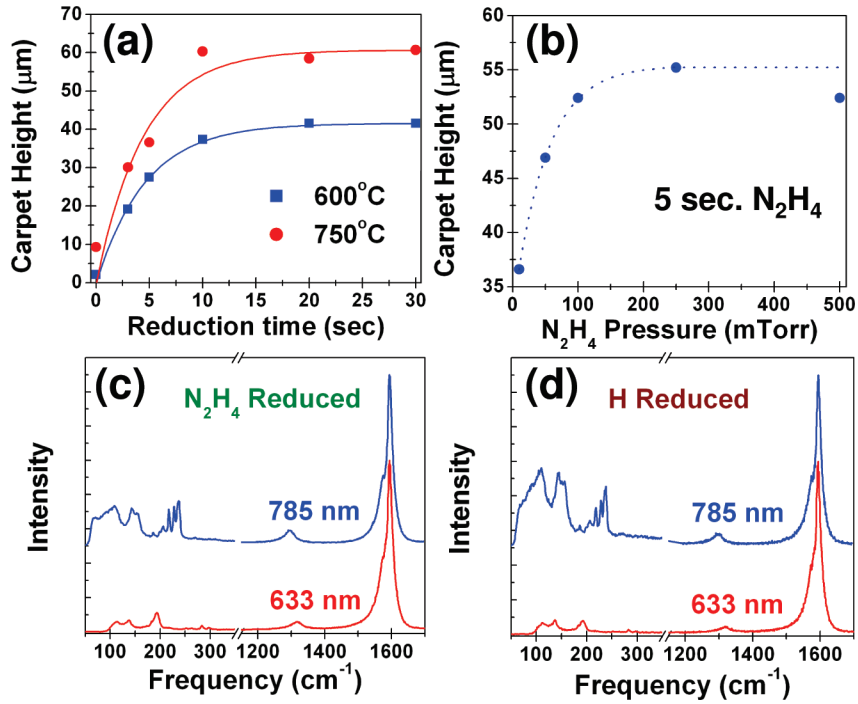

Figure 3. (a) Measured carpet height (average) as a function of total reduction time utilizing 10 mTorr N_2H_4 at two temperatures of 600 and 750 °C. (b) Measured carpet height as a function of N_2H_4 partial pressure for a 5 s exposure of N_2H_4 at 750 °C. (c,d) Raman spectra from 633 and 785 nm excitations of (c) a SWNT array grown following a 30 s exposure to 10 mTorr N_2H_4 at 750 °C, and (d) a SWNT array grown following a 30 s exposure to atomic hydrogen at 750 °C.

In order to investigate the potential of N_2H_4 as a reducing agent, the N_2H_4 partial pressure and exposure were varied in order to study the effect this has on the resulting SWNT array growth. Since the reduction and growth occurs in a closed system, we utilize the height measurement of the vertically aligned SWNT array (or carpet) in order to monitor the effectiveness of the reduction process. Significant work has been performed to establish that a catalyst particle will not be catalytically active until it is fully reduced into a metallic state.[26] Therefore, the measurement of the carpet height is a test of the effectiveness of the reduction process. Furthermore, the growth that occurs when no reducing agent is introduced into the reactor is nonuniform, occurring mostly or only at the edges of the growth substrate and less than 10 μm tall even where growth does occur. From Figure 2a, it is clear that the array that is grown is also less aligned due to having a substantially lower density. It is conceivable that within the 15 min exposure to high-temperature conditions in the presence of 1.4 Torr H_2, some of the most easily reduced catalyst will be activated and begin to grow nanotubes. However, this establishes a lower limit for comparison of carpet height between growth from a catalyst layer that has not been reduced *versus* a catalyst layer that has been fully reduced. Figure 3a shows the dependence of the carpet height on the exposure to 10 mTorr N_2H_4 at two different reduction/growth temperatures, with all growths carried out for a total of 15 min. From the applied fit, it is apparent that the carpet height as a function of N_2H_4 reduction time obeys a simple exponential decay function of the form:

$$H(t) = H_{max}(1 - \exp(-t/\tau))$$

where t is the N_2H_4 exposure time and τ represents a characteristic time for activation of a metal-oxide particle to a catalytically active metal particle. The finite values of carpet height in Figure 3a at $t = 0$ s represent the average measurable carpet height only over the spots on the substrate where growth is observed and not the height of a uniform carpet that is observed with $t > 0$ s. Therefore, for practical fitting reasons, the fits are extrapolated to zero height (*i.e.*, $H(0) = 0$ μm) without N_2H_4 exposure. The measured characteristic activation time constants from the applied fits are $\tau = 4.44 \pm 0.3$ s (750 °C) and $\tau = 4.61 \pm 0.1$ s (600 °C). This suggests that the hydrazine exposure at 750 °C more rap-

idly reduces the catalyst, even though the time constant associated with reduction at lower temperatures (600 °C) is not significantly different. As a result, as little as 10 mTorr of hydrazine is effective at reducing a thin catalyst layer over the range of temperatures one can utilize for carbon nanotube growth. It is also apparent from Figure 3a that the maximum height (with full catalyst reduction) is different for growth at temperatures of 600 and 750 °C. This was also observed in temperature-dependent studies of aligned carbon nanotube growth using similar conditions, but atomic hydrogen exposure for catalyst reduction.[27] This is attributed to slower kinetics during the addition of carbon to a growing nanotube at low temperatures, as this results in the formation of many nanotubes having additional walls and an overall slower rate of growth.[28] Nonetheless, the reduction process appears efficient at low temperatures and is a subject that will be revisited at a later point in this paper.

In addition to varying the N_2H_4 exposure time, we also investigated the dependence of the carpet height on the N_2H_4 partial pressure for a brief exposure (5 s) that is ineffective for full catalyst reduction, as evidenced by Figure 3a. The partial pressure was adjusted as described previously by modifying the opening of the vacuum seal on the hydrazine flask until the total system pressure stabilized. Mass spectrometry performed *in situ* downstream of the reaction was utilized as a means to identify the presence of N_2H_4 and whether the N_2H_4 partial pressure was stable. The pressure dependence of the carpet height on a brief N_2H_4 exposure is shown in Figure 3b. Again, the data appear to follow a curve describing exponential decay, with full carpet growth (~55 μm) observed after only 5 s of 0.2 Torr partial pressure N_2H_4 exposed to the catalyst at 750 °C. It should be noted that the N_2H_4 partial pressure is stabilized before rapid insertion of the catalyst and support into the hot reactor. This means that the catalyst is being reduced during substrate heating, depending on how rapidly the substrate absorbs the infrared radiation emitted by the tube furnace. The concept of low-temperature reduction will be presented at a later point; however, it is a substantial improvement to a vapor transport growth process to have the ability to reduce the catalyst quickly upon insertion into the reactor, minimizing any ripening effects or other dynamic processes which may inhibit selective or controllable growth.

Although monitoring the carpet height is a good diagnostic, it is important to establish that two different processes believed to only reduce the catalyst are not leading to a substantially different makeup of SWNTs in the carpets. In order to characterize and compare carpets grown *via* atomic hydrogen reduction to carpets grown *via* hydrazine reduction, Raman spectroscopy is performed on an exposed side of the carpet, as shown in Figure 3c,d. Raman spectroscopy is incredibly useful in its ability to characterize the "quality" of the graphitization of the nanotubes (D and G peak ratio) as well as a crude insight into nanotube diameters present in the sample. Analysis of Figure 3c,d indicates G/D ratios of 26.3 (633 nm) and 15.1 (785 nm) for SWNT grown from atomic hydrogen reduced catalyst, whereas ratios for nanotubes grown *via* hydrazine-reduced catalyst are 23.0 (633 nm) and 14.3 (785 nm). In other words, the quality measured by Raman spectroscopy is very similar between the growths where different reduction techniques are utilized. In addition to the D and G peaks, the lower frequency radial breathing modes (RBM) are diameter-dependent and allow one to make a crude judgment regarding the range of SWNT diameters present in the carpets. As is clear from Figure 3c,d, the general range of SWNT diameters, including specific breathing modes, is nearly identical in the two cases. One striking feature of the breathing modes is the substantial number of modes present near the cutoff filter for the lower excitation energy spectra. This indicates the presence of many larger-diameter SWNTs (1.5−2.5 nm), which is a feature unique to this water-assisted growth process. In any case, these results emphasize that the general makeup of nanotubes in terms of quality and the presence of RBMs is generally independent of the reduction process itself. As a result, this allows us to bypass the detailed SWNT characterization (provided elsewhere[27,29]) and focus on the specific aspects of hydrazine reduction relevant to this study.

The Raman results in Figure 3c,d as well as the general similarities in the carpets between reduction with N_2H_4 and atomic hydrogen raise a fundamental question regarding the initial state of the catalyst layer supporting growth. It is widely believed that the deposited metal catalyst layer forms a reasonably smooth, uniform layer on the catalyst support (Al_2O_3).[18] Upon reduction, this layer is believed to break into numerous small nucleation sites that will eventually yield SWNT growth, with particle sizes determined by factors such as the makeup of the incoming feedstock gases, and the rate at which reduction occurs. In order to understand the response of the catalyst layer to the different reduction conditions considered, we performed transmission electron microscope (TEM) imaging of the catalyst layers under the different reduction conditions. Images of the catalyst layer under the reduction conditions utilized in this work are shown in Figure 4, with accompanying inset histograms depicting metal-oxide particle size distributions. In order to prepare the samples for imaging, the catalyst-coated substrate is hand-polished from the back side until it is ~10 μm in thickness. Following this, the chip is further ion-milled at a low angle from the back side until it is perforated, thereby forming a small hole around which plan-view TEM imaging occurs. The conditions relevant to this study include four specific cases, shown in Figure 4: (i) an as-deposited layer of Fe, (ii) a catalyst layer reduced

with H_2, (iii) a catalyst layer reduced with atomic hydrogen, and (iv) a catalyst layer reduced with N_2H_4. All other conditions in (ii−iv) were identical, including a 30 s exposure to a reduction environment at a temperature of 750 °C. The catalyst layers for all experiments were e-beam deposited at the same time, meaning that any sample variation due to slight differences in the evaporation process is bypassed, allowing us to only focus on effects occurring due to the exposure of the catalyst layer to the reduction environment.

Upon inspection of Figure 4, a striking aspect of the catalyst layer is the appearance of Fe particle formation on the Al_2O_3 support in the as-deposited layer (Figure 4a). Histograms indicate that typical metal-oxide particle sizes correlate reasonably to the SWNT population observed in the growth process, assuming the metal-oxide particle is reduced prior to growth. This provides crucial insight into the growth process by emphasizing that the primary role of the reduction environment is not to regulate the formation of the particle size distribution from a uniformly coated metal layer. This means that the particle formation, to first order, occurs during deposition. This is an important point to make and is likely the reason why the "super-growth" process is highly sensitive to the thickness of the catalyst layer.[30,31] In all images shown in Figure 4, the metal particles are converted back into Fe_2O_3 during the substantial air exposure that occurs between reduction and TEM imaging experiments. Therefore, the actual catalyst particle size relevant to SWNT growth is likely ~30−40% smaller than the sizes shown in Figure 4 and depicted through inset histograms. By comparison of Figure 4a,b, it is evident that exposure of the catalyst layer to a reduction environment consisting only of H_2 as the reducing agent results in particle coarsening, even after only 30 s. This coarsening effect likely occurs due to Ostwald ripening at temperatures which support high atomistic mobility.[17] However, when atomic hydrogen is utilized (Figure 4c) as the reduction agent, particles apparently form with sizes that are on average slightly larger than those in the as-deposited layer, but appearing compact in nature. Looking closely, there is a wide distribution of particle sizes that would represent a distribution of large-diameter nanotubes consistent with what has been characterized previously assuming the particles were shrunk to fit their metallic (not metal-oxide) size. The drawback to this reduction process is the dependence of the atomic hydrogen exposure on the distance of the sample from the hot filament. In order to investigate this effect, additional TEM imaging performed emphasizes significantly different catalyst particle size distribution at an opposite end of the chip. This emphasizes the drawback to utilizing the hot filament as a scalable technique and further bolsters the need for a scalable, uniform process such as hydrazine reduction. On the basis of size measurements of 300 particles from each reduction condition corresponding to the inset histograms, the average particle sizes measured are (a) 4.9 nm (as-deposited), (b) 6.6 nm (H_2 reduced), (c) 5.0 nm (H reduced), and (d) 3.9 nm (N_2H_4 reduced). Although the average particle size is slightly smaller when utilizing N_2H_4 reduction, the emergence of a significant number of particles having diameters larger than the range of as-deposited particles (*i.e.*, with $d >$ 6−7 nm) is not apparent, suggesting that this reduction process best preserves the initial particle size distribution for growth. This emphasizes a point that is already well-accepted in the literature: the catalyst prereduction step is fundamental to maintaining a given catalyst particle size.[13−16] This makes any effort to achieve

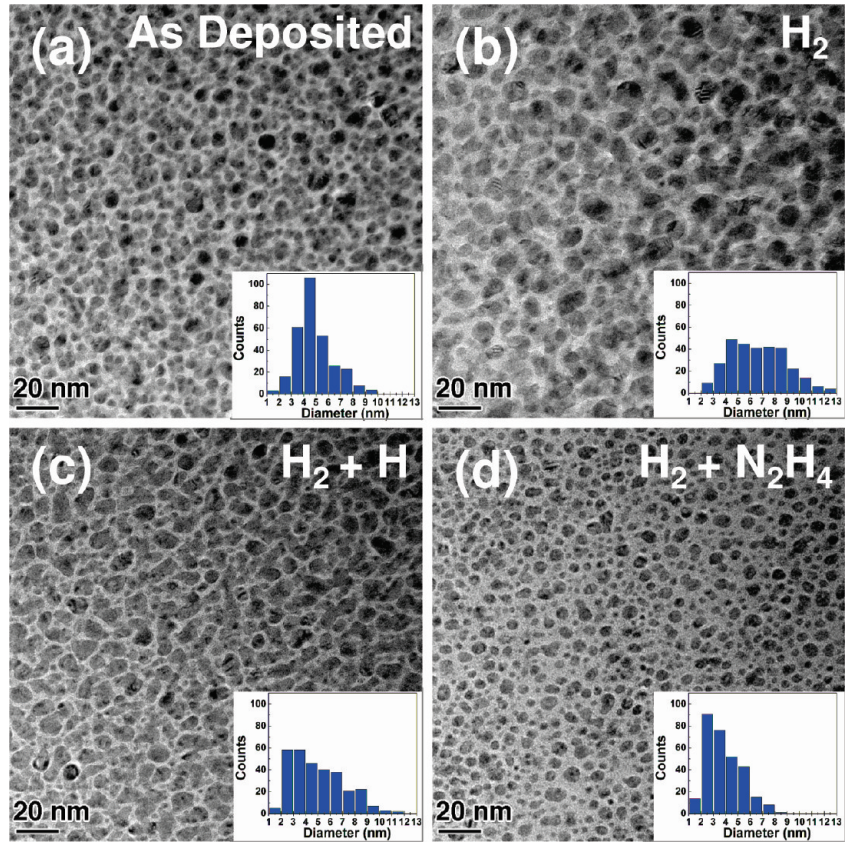

Figure 4. Plan-view TEM images of 0.5 nm thick Fe catalyst layers deposited onto an alumina supporting layer and exposed to different reduction conditions. (a) As-deposited layer of Fe catalyst, showing the formation of particles during the deposition process. (b) Catalyst layer exposed to 1.4 Torr H_2 as the reduction condition for 30 s at 750 °C, (c) catalyst layer exposed to atomic hydrogen for 30 s, produced in 1.4 Torr H_2 with a hot filament at 750 °C, and (d) catalyst layer exposed to 10 mTorr N_2H_4 for 30 s at 750 °C, in addition to a background of 1.4 Torr H_2. Scale bars in all images are 20 nm, and all panels have inset histograms depicting size distributions of particles from $N = 300$ total particles.

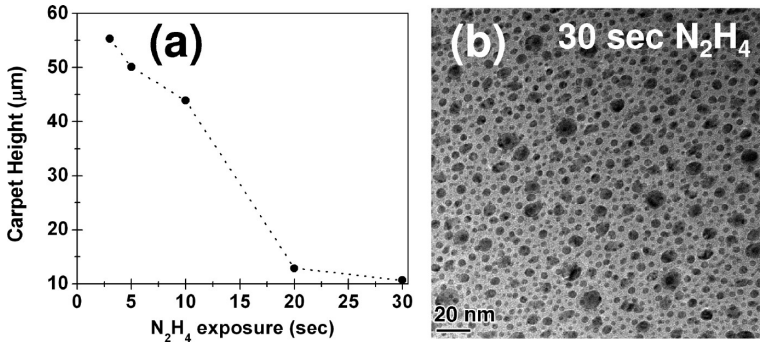

Figure 5. (a) Measured carpet height (average) as a function of 0.5 Torr partial pressure N_2H_4 exposure at 750 °C. (b) Plan-view TEM image of the catalyst layer following a 30 s exposure to 0.5 Torr N_2H_4.

selective SWNT growth sensitive not only to the initial size distribution of the particles but also to the reduction conditions utilized before SWNT nucleation takes place. In Figure 4, it is clear that rapid reduction with N_2H_4 results in a particle size distribution most closely correlated to the starting particle size distribution, and histograms depicting particle size distributions for the other two reduction techniques indicate a significant emergence of coarsened particles having diameters larger than the as-deposited catalyst layer. Therefore, not only is the catalyst size distribution sensitive to reduction conditions, but the rapid catalyst reduction obtained from N_2H_4 vapor exposure is best-geared toward selective growth processes.

Although N_2H_4 reduction, particularly with low N_2H_4 partial pressures, appears to be highly beneficial for catalyst reduction, we find that too much N_2H_4 exposure for extended periods of time is not beneficial. In Figure 5a, a plot of carpet height as a function of reduction time with 0.5 Torr partial pressure N_2H_4 (~50 times more N_2H_4 than utilized previously) emphasizes the sensitivity of growth to extended exposure involving too much N_2H_4. Full reduction appears to take place quickly upon rapid insertion of the sample into the furnace (<3 s), as evidenced by the maximum carpet height achieved in the briefest possible exposure time. However, as the exposure time is increased (even at 5 s), the resulting height of the carpet consistently decreases. To better understand this effect, we imaged the catalyst layer following exposure to 30 s N_2H_4 (0.5 Torr partial pressure) at 750 °C, shown in Figure 5b. Compared to images presented in Figure 4, one can clearly observe the emergence of large particles (~15−20 nm) and the overall "shrinking" of the smaller particles. Although this does not explain the falloff in growth with greater N_2H_4 exposure, it is analogous to the rapid ripening effect observed without the presence of H_2O during growth, as H_2O is expected to hydroxylate the surface and reduce the rate of catalyst ripening.[17,27] One possible explanation for this effect is that N_2H_4 is known to attack surface hydroxyl radicals,[32] which would result in catalyst ripening behavior in the early stages of nucleation analogous to the case when no water was utilized during the growth process. In such a case, the terminal carpet height achieved is ~10 μm in these growth conditions, similar to that presented in Figure 5b for a 30 s exposure to 0.5 Torr N_2H_4.

Finally, in the framework of maintaining the most controllable and selective growth conditions, we performed experiments where reduction and growth occur separately and at different temperatures. The principle of this is based upon the fact that dynamic catalyst behavior will be impeded at low temperatures, yielding a preserved catalyst layer which will uniformly nucleate SWNTs upon rapid insertion into a preheated furnace. We now revisit data from Figure 3a, which emphasize that the characteristic activation time constant describing the catalyst reduction process does not appear to have a substantial temperature dependence over the range of temperatures in which SWNT growth is typically achieved. Therefore, this emphasizes the possibility that low-temperature reduction is another potential advantage in utilizing a N_2H_4 vapor transport reduction process. The results of this experiment are presented in Figure 6a, utilizing 0.25 Torr N_2H_4 partial pressure in experiments performed at a reduction temperature lower than that of the growth temperature. In order to compare the effectiveness of the reduction process at low temperatures, an identical experiment is also carried out using hot filament (atomic hydrogen) reduction. For the case of N_2H_4 reduction, the chip is rapidly inserted into the furnace under flow of H_2 and H_2O for 10 s, after which the N_2H_4 valve is opened and 20 s of N_2H_4 exposure at that temperature occurs before the sample is removed and the N_2H_4 is turned off. For the case of atomic hydrogen reduction, the hot filament is energized and the chip is placed inside the heated furnace for a total of 30 s, after which the chip is removed and the hot filament turned off. Following removal from the low-temperature reduction environment, the sample is immediately moved into an isolated vacuum until the furnace heats to the growth temperature. Immediately apparent from Figure 6a is the ability to reduce the catalyst layer at low temperatures (<400 °C) with N_2H_4, yielding a carpet that grows to the full length expected for the growth conditions utilized. However, comparing this result with that obtained from hot filament reduction emphasizes a difference of over 200 °C in the lowest prereduction temperature that is effective in the growth of a full-length SWNT carpet. It should be noted that "NU" on the bottom of the vertical axis in Figure 6 represents the nonuniform growth that typically is representative of the growth observed when no reduction technique is utilized (either atomic hydrogen or N_2H_4). Another interesting feature associated with Figure 6a is the observation that the hot filament reduction process is only effective in the temperature range in which efficient

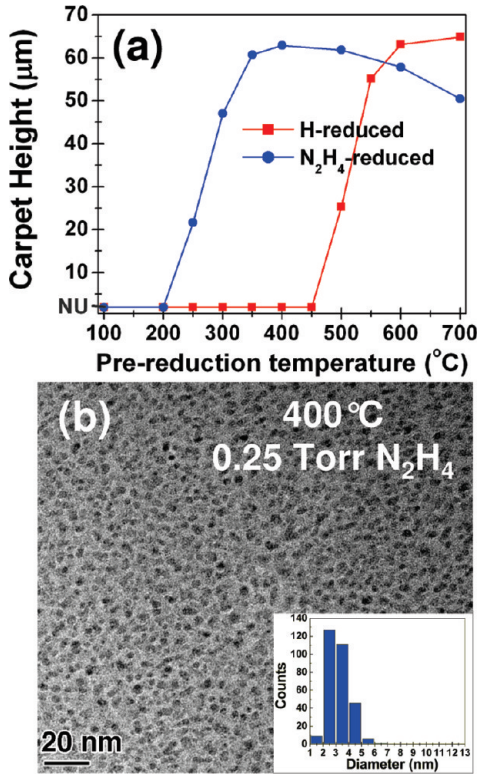

Figure 6. (a) Carpet height (average) dependence of a low-temperature prereduction prior to growth. For the case of N_2H_4 reduction, the prereduction involves 10 s of heating, followed by 20 s of 0.25 Torr N_2H_4 vapor exposure. For the case of atomic hydrogen reduction, the prereduction involves 30 s of atomic hydrogen exposure at a set prereduction temperature. Between prereduction and growth, the sample is moved into vacuum and the carbon feedstock is turned on. (b) Plan-view TEM image of catalyst following N_2H_4 reduction at 400 °C under conditions described in part (a), with inset histogram depicting particle size distributions from $N = 300$ total particles.

growth is observed (>20 μm), whereas the hydrazine reduction process is efficient at over 200 °C lower in temperature. In order to better understand low-temperature catalyst reduction with N_2H_4, we performed further imaging on a catalyst layer exposed to a 25 s treatment (identical to that in Figure 6a) upon rapid insertion to a furnace heated to 400 °C. The resulting catalyst layer is shown in Figure 6b, with an accompanying inset histogram. First of all, it is evident when comparing Figure 6b to Figure 4a that the catalyst layer treated at 400 °C involves a slightly different distribution of catalyst particle sizes that are smaller than the particles formed during catalyst deposition. Furthermore, there is no indication of ripening phenomena occurring during this reduction process, which is typically evidenced by the emergence of large particles and a distribution of shrinking smaller particles. In this case, the average particle size is 3.2 nm with a relatively narrow distribution (only a few metal-oxide particles observed with $d > 5$ nm). In addition, similar catalyst imaging experiments were performed on a catalyst layer exposed to three times longer N_2H_4 exposure at room temperature, and absolutely no change between the as-deposited sample and the room temperature N_2H_4 treated sample is evident. This means that the low-temperature reduction process results in catalyst mobility that is responsible for the rearrangement of the catalyst on the surface into smaller islands, even though the temperature is too low to promote the onset of Ostwald ripening. As a result, the ability to fully reduce the catalyst at a temperature significantly lower than typical SWNT growth temperatures allows an optimal level of control of the catalyst in the reduction stage, which is likely most important for high-density SWNT array nucleation, particularly where any selectivity is desired. In addition, such rapid reduction of metal-oxide catalyst at low temperatures provides a route that strongly appeals toward the many research efforts to find new ways to grow SWNT at low temperatures—a concept that could strongly impact chirality selective SWNT growth techniques, as well as the cost and availability of large-scale industrially produced SWNT material.

In closing, this work, describing an efficient technique for rapid reduction of metal-oxide particles *via* vapor transport processes, is not carbon-nanotube-specific but also relevant to a growing effort to utilize metal particles for catalysis of a number of new and exciting nanostructured materials. Metal-oxide layers supporting high-density SWNT growth are only one of the many relevant emerging systems and among one of the most sensitive to the reduction process as they are vulnerable to Ostwald ripening effects due to a close-packed arrangement of particles having high strain energies. Nonetheless, the scalable and incredibly efficient approach described in this study could benefit any large-scale process where a metal-oxide particle of any size or density on a surface must be reduced in order to reveal its catalytic nature in the synthesis of a particular nanostructured object. This broadens the applicability of this method to numerous growth processes which focus on the synthesis of a wide variety of unique materials which each have significant potential for impacting important applications in the future.

CONCLUSIONS

We present here an efficient technique for rapid reduction of layers composed of metal-oxide catalytic particles utilizing hydrazine vapor. Our results indicate that the use of 10 mTorr N_2H_4 for less than 15 s is sufficient to reduce catalyst supporting the growth of vertically aligned SWNT, whereas greater N_2H_4 partial pressures result in reduction occurring in less than 3 s of N_2H_4 exposure. Compared to the use of the hot filament, N_2H_4 reduction occurs more quickly, best preserves the initial distribution of particle sizes, and can be scalable for large-area reduction unlike the hot filament. On the basis of this work, hydrazine vapor reduction appears to be the

most efficient and scalable technique for catalyst reduction for high-density SWNT growth and is likely to be applicable to other forms of surface-supported catalysis from metal particles, as well.

METHODS

The hydrazine utilized for these experiments was purchased from Sigma Aldrich (hydrazine, anhydrous, 98%) and loaded directly into the O-ring sealed flask with Teflon fittings in a fume hood. Once loaded, the flask was attached to the reactor system upstream of the reaction chamber as simply illustrated in Figure 1. A detailed photograph of the reactor system with a label indicating gas flow direction is also presented in the Supporting Information. To open the N_2H_4 flask, a knob is turned on the top of the flask which modifies the opening of an O-ring fitting. Exposure to the reaction gas flow is achieved by opening a two-way valve (Swagelok item 6LVV-DPF222P-C, located on the right-hand side of the flask in Figure S1 in Supporting Information). This valve was specifically chosen to minimize dead space as it opens directly into a channel in which the reaction gases (H_2, C_2H_2, H_2O, as shown in Figure S1 in Supporting Information) are flowing. Therefore, precise exposures of N_2H_4 can be achieved, yielding accuracy in measurements of growth from well-defined N_2H_4 exposure times and concentrations. In order to monitor the partial pressure of N_2H_4, a pressure gauge (100 Torr MKS Baratron) directly downstream of the reaction chamber was monitored while the valve was opened and the black knob on the N_2H_4 flask was slowly turned, further opening the O-ring seal and exposing N_2H_4 vapor to the reactor. The partial pressure of N_2H_4 is determined from the assumption of an ideal gas mixture (*i.e.*, $P_{TOT} = P_{H_2+H_2O+C_2H_2} + P_{N_2H_4}$) by the measurement of the total pressure difference before and after the N_2H_4 flask is opened and allowed to reach equilibrium. After a desired pressure was achieved (reaction gases + N_2H_4), mass spectrometry conducted further downstream was utilized to confirm the presence of N_2H_4 and to support that the partial pressure had stabilized. For these experiments, mass spectrometry is utilized only for analysis of reaction gas mixture products and their relative abundance since the mass spectrum (see Supporting Information) is complicated by ionization cross sections and cracking patterns. Utilizing this process, the partial pressure of N_2H_4 was found to be controllable between 10 and 500 mTorr—a wide range amenable to the study conducted in this work. In order to control the exposure time of the N_2H_4, LabView software was developed to control and operate a Fieldpoint relay to control a 12 V DC signal to activate the valve. A properly vented scroll pump was utilized to maintain a constant vacuum during all processes of reduction, annealing, or growth. Further details of the experimental design for the reaction system beyond that described for N_2H_4 exposure and the specific conditions utilized in the growth process are located elsewhere.[27] Following growth, carpet height analysis was carried out with an FEI Quanta 400 environmental scanning electron microscope, and catalyst layer imaging after exposure to annealing conditions was performed with an FEI field emission transmission electron microscope/scanning transmission electron microscope (S/TEM) (80-300 Titan).

Acknowledgment. The authors acknowledge D. Natelson for use of equipment for catalyst deposition. Special thanks to S. Ripley, M. Pasquali, B. Maruyama, and N. Alvarez for discussions. C.L.P. and R.H.H. acknowledge support from the Lockheed Martin Advanced Nanotechnology Center for Excellence at Rice University (LANCER). S.M.K. and E.A.S. acknowledge support from the National Science Foundation Grant No. DMR-0606395.

Supporting Information Available: Additional experimental details and TEM imaging of catalyst layers provided. This material is available free of charge *via* the Internet at http://pubs.acs.org.

REFERENCES AND NOTES

1. Morales, A. M.; Lieber, C. M. A Laser Ablation Method for the Synthesis of Crystalline Semiconductor Nanowires. *Science* **1998**, *279*, 208–211.
2. Kamins, T. I.; Williams, R. S.; Basile, D. P.; Hesjedal, T.; Harris, J. S. Ti-Catalyzed Si Nanowires by Chemical Vapor Deposition: Microscopy and Growth Mechanisms. *J. Appl. Phys.* **2001**, *89*, 1008–1016.
3. Wang, Y.; Schmidt, V.; Senz, S.; Gosele, U. Epitaxial Growth of Silicon Nanowires Using an Aluminum Catalyst. *Nat. Nanotechnol.* **2006**, *1*, 186–189.
4. Kim, B. J.; Tersoff, J.; Kodambaka, S.; Reuter, M. C.; Stach, E. A.; Ross, F. M. Kinetics of Individual Nucleation Events Observed in Nanoscale Vapor-Liquid-Solid Growth. *Science* **2008**, *322*, 1070–1073.
5. Gao, P. X.; Ding, Y.; Wang, Z. L. Crystallographic Orientation-Aligned ZnO Nanorods Grown by a Tin Catalyst. *Nano Lett.* **2003**, *3*, 1315–1320.
6. Lourie, O. R.; Jones, C. R.; Bartlett, B. M.; Gibbons, P. C.; Ruoff, R. S.; Buhro, W. E. CVD Growth of Boron Nitride Nanotubes. *Chem. Mater.* **2000**, *12*, 1808–1810.
7. Murakami, Y.; Chiashi, S.; Miyauchi, Y.; Minghui, H.; Ogura, M.; Okubo, T.; Maruyama, S. Growth of Vertically Aligned Single-Walled Carbon Nanotube Films on Quartz Substrates and Their Anisotropy. *Chem. Phys. Lett.* **2004**, *385*, 298–303.
8. Hata, K.; Futaba, D. N.; Mizuno, K.; Namai, T.; Yumura, M.; Iijima, S. Water Assisted Highly Efficient Synthesis of Impurity Free Single-Walled Carbon Nanotubes. *Science* **2004**, *206*, 1362–1364.
9. Maruyama, S.; Einarsson, E.; Murakami, Y.; Edamura, T. Growth Process of Vertically Aligned Single-Walled Carbon Nanotubes. *Chem. Phys. Lett.* **2005**, *403*, 320–323.
10. Eres, G.; Kinkhabwala, A. A.; Cui, H.; Geohegan, D. B.; Puretzky, A. A.; Lowndes, D. H. Molecular Beam-Controlled Nucleation and Growth of Vertically Aligned Single-Wall Carbon Nanotube Arrays. *J. Phys. Chem. B* **2005**, *109*, 16684–16694.
11. Puretzky, A. A.; Geohegan, D. B.; Jesse, S.; Ivanov, I. N.; Eres, G. *In Situ* Measurements and Modeling of Carbon Nanotube Array Growth Kinetics During Chemical Vapor Deposition. *Appl. Phys. A: Mater. Sci. Process.* **2005**, *81*, 223–240.
12. Xu, Y.; Flor, E.; Kim, M. J.; Hamadani, B.; Schmidt, H.; Smalley, R. E.; Hauge, R. H. Vertical Array Growth of Small Diameter Single-Walled Carbon Nanotubes. *J. Am. Chem. Soc.* **2006**, *128*, 6560–6561.
13. Pint, C. L.; Pheasant, S. T.; Pasquali, M.; Coulter, K. E.; Schmidt, H. K.; Hauge, R. H. Synthesis of High Aspect-Ratio Carbon Nanotube "Flying Carpets" from Nanostructured Flake Substrates. *Nano Lett.* **2008**, *8*, 1879–1883.
14. Chen, Y.; Ciuparu, D.; Lim, S.; Yang, Y.; Haller, G. L.; Pfefferle, L. Synthesis of Uniform Diameter Single-Wall Carbon Nanotubes in Co-MCM-41: Effects of the Catalyst Prereduction and Nanotube Growth Temperatures. *J. Catal.* **2004**, *225*, 453–465.
15. Pisana, S.; Cantoro, M.; Parvez, A.; Hofmann, S.; Ferrari, A. C.; Robertson, J. The Role of Precursor Gases on the Surface Restructuring of Catalyst Films during Carbon Nanotube Growth. *Physica E* **2007**, *37*, 1–5.
16. Nessim, G. D.; Hart, A. J.; Kim, J. S.; Acquaviva, D.; Oh, J.; Morgan, C. D.; Seita, M.; Leib, J. S.; Thompson, C. V. Tuning of Vertically-Aligned Carbon Nanotube Diameter and Arial Density through Catalyst Pre-Treatment. *Nano Lett.* **2008**, *8*, 3587–3593.
17. Amama, P. B.; Pint, C. L.; McJilton, L.; Kim, S. M.; Stach, E. A.; Murray, T.; Hauge, R. H.; Maruyama, B. Role of Water in Super Growth of Single-Walled Carbon Nanotube Carpets. *Nano Lett.* **2009**, *9*, 44–49.
18. Dupuis, A.-C. The Catalyst in the CCVD of Carbon Nanotubes: A Review. *Prog. Mater. Sci.* **2005**, *50*, 929–961.

19. Xu, Y.-Q.; Flor, E.; Schmidt, H.; Smalley, R. E.; Hauge, R. H. Effect of Atomic Hydrogen and Active Carbon Species in 1 mm Vertically Aligned Single-Walled Carbon Nanotube Growth. *Appl. Phys. Lett.* **2006**, *89*, 123116–123118.
20. Futaba, D. N.; Hata, K.; Yamada, T.; Hiraoka, T.; Hayamizu, T.; Kakudate, Y.; Tanaike, O.; Hatori, H.; Yumura, M.; Iijima, S. Shape-Engineerable and Highly Densely Packed Single-Walled Carbon Nanotubes and their Application as Super-Capacitor Electrodes. *Nat. Mater.* **2006**, *5*, 987–994.
21. Thong, J. T. L.; Oon, C. H.; Eng, W. K.; Zhang, W. D.; Gan, L. M. High-Current Field Emission from a Vertically Aligned Carbon Nanotube Field Emitter Array. *Appl. Phys. Lett.* **2001**, *79*, 2811.
22. Majumder, M.; Chopra, N.; Andrews, R.; Hinds, B. J. Nanoscale Hydrodynamics Enhanced Flow in Carbon Nanotubes. *Nature* **2005**, 44.
23. Holt, J. K.; Park, H. G.; Wang, Y.; Stadermann, M.; Artyukhin, A. B.; Grigoropoulos, C. P.; Noy, A.; Bakajin, O. Fast Mass Transport Through Sub-2-Nanometer Carbon Nanotubes. *Science* **2006**, *312*, 1034–1037.
24. Xiao, L.; Chen, Z.; Feng, C.; Liu, L.; Bai, Z.; Wang, Y.; Qian, L.; Zhang, Y.; Li, Q.; Jiang, K.; Fan, S. Flexible, Stretchable, Transparent Carbon Nanotube Thin Film Loudspeakers. *Nano Lett.* **2008**, *8*, 4539–4545.
25. Larjo, J.; Koivikka, H.; Li, D.; Hernberg, R. Atomic Hydrogen Mapping in Hot Filament Chemical Vapor Deposition. *Appl. Opt.* **2001**, *40*, 765–769.
26. Mattevi, C.; Wirth, C. T.; Hoffman, S.; Blume, R.; Cantoro, M.; Ducati, C.; Cepek, C.; Knop-Gericke, A.; Milne, S.; Castellarin-Cudia, C. *In-Situ* X-ray Photoelectron Spectroscopy Study of Catalyst-Support Interactions and Growth of Carbon Nanotube Forests. *J. Phys. Chem. C* **2008**, *112*, 12207–12213.
27. Pint, C. L.; Pheasant, S. T.; Parra-Vasquez, A. N. G.; Horton, C.; Xu, Y.; Hauge, R. H. Investigation of Optimal Parameters for Oxide-Assisted Growth of Vertically Aligned Single-Walled Carbon Nanotubes. *J. Phys. Chem. C* **2009**, *113*, 4125–4133.
28. Wood, R. F.; Pannala, S.; Wells, J. C.; Puretzky, A. A.; Geohegan, D. B. Simple Model of the Interrelation Between Single- and Multiwall Carbon Nanotube Growth Rates for the CVD Process. *Phys. Rev. B* **2007**, *75*, 235446.
29. Pint, C. L.; Pheasant, S. T.; Nicholas, N.; Horton, C. C.; Hauge, R. H. The Role of the Substrate Surface Morphology and Water in the Growth of Vertically Aligned Single-Walled Carbon Nanotubes. *J. Nanosci. Nanotechnol.* **2008**, *8*, 6158.
30. Noda, S.; Hasegawa, K.; Sugime, H.; Kakehi, K.; Zhang, Z.; Maruyama, S.; Yamaguchi, Y. Millimeter-Thick Single-Walled Carbon Nanotube Forests: Hidden Role of Catalyst Support. *Jpn. J. Appl. Phys.* **2007**, *46*, 399–401.
31. Zhao, B.; Futaba, D. N.; Yasuda, S.; Akoshima, M.; Yamada, T.; Hata, K. Exploring Advantages of Diverse Carbon Nanotube Forests with Tailored Structures Synthesized by Supergrowth from Engineered Catalysts. *ACS Nano* **2009**, *3*, 108–114.
32. Harris, G. W.; Atkinson, R.; Pitts, J. N. Kinetics of the Reactions of the OH Radical with Hydrazine and Methylhydrazine. *J. Phys. Chem.* **1979**, *83*, 2557–2559.